BELLE-CONF-0528
LP2005-163
EPS05-502

Search for Direct CP Violation in Three-Body Charmless $B^{\pm} \to K^{\pm}\pi^{\pm}\pi^{\mp}$ Decay

K. Abe,[9] K. Abe,[47] I. Adachi,[9] H. Aihara,[49] K. Aoki,[23] K. Arinstein,[2] Y. Asano,[54] T. Aso,[53] V. Aulchenko,[2] T. Aushev,[13] T. Aziz,[45] S. Bahinipati,[5] A. M. Bakich,[44] V. Balagura,[13] Y. Ban,[36] S. Banerjee,[45] E. Barberio,[22] M. Barbero,[8] A. Bay,[19] I. Bedny,[2] U. Bitenc,[14] I. Bizjak,[14] S. Blyth,[25] A. Bondar,[2] A. Bozek,[29] M. Bračko,[9,21,14] J. Brodzicka,[29] T. E. Browder,[8] M.-C. Chang,[48] P. Chang,[28] Y. Chao,[28] A. Chen,[25] K.-F. Chen,[28] W. T. Chen,[25] B. G. Cheon,[4] C.-C. Chiang,[28] R. Chistov,[13] S.-K. Choi,[7] Y. Choi,[43] Y. K. Choi,[43] A. Chuvikov,[37] S. Cole,[44] J. Dalseno,[22] M. Danilov,[13] M. Dash,[56] L. Y. Dong,[11] R. Dowd,[22] J. Dragic,[9] A. Drutskoy,[5] S. Eidelman,[2] Y. Enari,[23] D. Epifanov,[2] F. Fang,[8] S. Fratina,[14] H. Fujii,[9] N. Gabyshev,[2] A. Garmash,[37] T. Gershon,[9] A. Go,[25] G. Gokhroo,[45] P. Goldenzweig,[5] B. Golob,[20,14] A. Gorišek,[14] M. Grosse Perdekamp,[38] H. Guler,[8] R. Guo,[26] J. Haba,[9] K. Hara,[9] T. Hara,[34] Y. Hasegawa,[42] N. C. Hastings,[49] K. Hasuko,[38] K. Hayasaka,[23] H. Hayashii,[24] M. Hazumi,[9] T. Higuchi,[9] L. Hinz,[19] T. Hojo,[34] T. Hokuue,[23] Y. Hoshi,[47] K. Hoshina,[52] S. Hou,[25] W.-S. Hou,[28] Y. B. Hsiung,[28] Y. Igarashi,[9] T. Iijima,[23] K. Ikado,[23] A. Imoto,[24] K. Inami,[23] A. Ishikawa,[9] H. Ishino,[50] K. Itoh,[49] R. Itoh,[9] M. Iwasaki,[49] Y. Iwasaki,[9] C. Jacoby,[19] C.-M. Jen,[28] R. Kagan,[13] H. Kakuno,[49] J. H. Kang,[57] J. S. Kang,[16] P. Kapusta,[29] S. U. Kataoka,[24] N. Katayama,[9] H. Kawai,[3] N. Kawamura,[1] T. Kawasaki,[31] S. Kazi,[5] N. Kent,[8] H. R. Khan,[50] A. Kibayashi,[50] H. Kichimi,[9] H. J. Kim,[18] H. O. Kim,[43] J. H. Kim,[43] S. K. Kim,[41] S. M. Kim,[43] T. H. Kim,[57] K. Kinoshita,[5] N. Kishimoto,[23] S. Korpar,[21,14] Y. Kozakai,[23] P. Križan,[20,14] P. Krokovny,[9] T. Kubota,[23] R. Kulasiri,[5] C. C. Kuo,[25] H. Kurashiro,[50] E. Kurihara,[3] A. Kusaka,[49] A. Kuzmin,[2] Y.-J. Kwon,[57] J. S. Lange,[6] G. Leder,[12] S. E. Lee,[41] Y.-J. Lee,[28] T. Lesiak,[29] J. Li,[40] A. Limosani,[9] S.-W. Lin,[28] D. Liventsev,[13] J. MacNaughton,[12] G. Majumder,[45] F. Mandl,[12] D. Marlow,[37] H. Matsumoto,[31] T. Matsumoto,[51] A. Matyja,[29] Y. Mikami,[48] W. Mitaroff,[12] K. Miyabayashi,[24] H. Miyake,[34] H. Miyata,[31] Y. Miyazaki,[23] R. Mizuk,[13] D. Mohapatra,[56] G. R. Moloney,[22] T. Mori,[50] A. Murakami,[39] T. Nagamine,[48] Y. Nagasaka,[10] T. Nakagawa,[51] I. Nakamura,[9] E. Nakano,[33] M. Nakao,[9] H. Nakazawa,[9] Z. Natkaniec,[29] K. Neichi,[47] S. Nishida,[9] O. Nitoh,[52] S. Noguchi,[24] T. Nozaki,[9] A. Ogawa,[38] S. Ogawa,[46] T. Ohshima,[23] T. Okabe,[23] S. Okuno,[15] S. L. Olsen,[8] Y. Onuki,[31] W. Ostrowicz,[29] H. Ozaki,[9] P. Pakhlov,[13] H. Palka,[29] C. W. Park,[43] H. Park,[18] K. S. Park,[43] N. Parslow,[44] L. S. Peak,[44] M. Pernicka,[12] R. Pestotnik,[14] M. Peters,[8] L. E. Piilonen,[56] A. Poluektov,[2] F. J. Ronga,[9] N. Root,[2] M. Rozanska,[29] H. Sahoo,[8] M. Saigo,[48] S. Saitoh,[9] Y. Sakai,[9] H. Sakamoto,[17] H. Sakaue,[33] T. R. Sarangi,[9] M. Satapathy,[55] N. Sato,[23] N. Satoyama,[42] T. Schietinger,[19] O. Schneider,[19] P. Schönmeier,[48] J. Schümann,[28] C. Schwanda,[12] A. J. Schwartz,[5] T. Seki,[51] K. Senyo,[23] R. Seuster,[8] M. E. Sevior,[22] T. Shibata,[31] H. Shibuya,[46]

J.-G. Shiu,[28] B. Shwartz,[2] V. Sidorov,[2] J. B. Singh,[35] A. Somov,[5] N. Soni,[35] R. Stamen,[9] S. Stanič,[32] M. Starič,[14] A. Sugiyama,[39] K. Sumisawa,[9] T. Sumiyoshi,[51] S. Suzuki,[39] S. Y. Suzuki,[9] O. Tajima,[9] N. Takada,[42] F. Takasaki,[9] K. Tamai,[9] N. Tamura,[31] K. Tanabe,[49] M. Tanaka,[9] G. N. Taylor,[22] Y. Teramoto,[33] X. C. Tian,[36] K. Trabelsi,[8] Y. F. Tse,[22] T. Tsuboyama,[9] T. Tsukamoto,[9] K. Uchida,[8] Y. Uchida,[9] S. Uehara,[9] T. Uglov,[13] K. Ueno,[28] Y. Unno,[9] S. Uno,[9] P. Urquijo,[22] Y. Ushiroda,[9] G. Varner,[8] K. E. Varvell,[44] S. Villa,[19] C. C. Wang,[28] C. H. Wang,[27] M.-Z. Wang,[28] M. Watanabe,[31] Y. Watanabe,[50] L. Widhalm,[12] C.-H. Wu,[28] Q. L. Xie,[11] B. D. Yabsley,[56] A. Yamaguchi,[48] H. Yamamoto,[48] S. Yamamoto,[51] Y. Yamashita,[30] M. Yamauchi,[9] Heyoung Yang,[41] J. Ying,[36] S. Yoshino,[23] Y. Yuan,[11] Y. Yusa,[48] H. Yuta,[1] S. L. Zang,[11] C. C. Zhang,[11] J. Zhang,[9] L. M. Zhang,[40] Z. P. Zhang,[40] V. Zhilich,[2] T. Ziegler,[37] and D. Zürcher[19]

(The Belle Collaboration)

[1]*Aomori University, Aomori*
[2]*Budker Institute of Nuclear Physics, Novosibirsk*
[3]*Chiba University, Chiba*
[4]*Chonnam National University, Kwangju*
[5]*University of Cincinnati, Cincinnati, Ohio 45221*
[6]*University of Frankfurt, Frankfurt*
[7]*Gyeongsang National University, Chinju*
[8]*University of Hawaii, Honolulu, Hawaii 96822*
[9]*High Energy Accelerator Research Organization (KEK), Tsukuba*
[10]*Hiroshima Institute of Technology, Hiroshima*
[11]*Institute of High Energy Physics, Chinese Academy of Sciences, Beijing*
[12]*Institute of High Energy Physics, Vienna*
[13]*Institute for Theoretical and Experimental Physics, Moscow*
[14]*J. Stefan Institute, Ljubljana*
[15]*Kanagawa University, Yokohama*
[16]*Korea University, Seoul*
[17]*Kyoto University, Kyoto*
[18]*Kyungpook National University, Taegu*
[19]*Swiss Federal Institute of Technology of Lausanne, EPFL, Lausanne*
[20]*University of Ljubljana, Ljubljana*
[21]*University of Maribor, Maribor*
[22]*University of Melbourne, Victoria*
[23]*Nagoya University, Nagoya*
[24]*Nara Women's University, Nara*
[25]*National Central University, Chung-li*
[26]*National Kaohsiung Normal University, Kaohsiung*
[27]*National United University, Miao Li*
[28]*Department of Physics, National Taiwan University, Taipei*
[29]*H. Niewodniczanski Institute of Nuclear Physics, Krakow*
[30]*Nippon Dental University, Niigata*
[31]*Niigata University, Niigata*
[32]*Nova Gorica Polytechnic, Nova Gorica*

[33]Osaka City University, Osaka
[34]Osaka University, Osaka
[35]Panjab University, Chandigarh
[36]Peking University, Beijing
[37]Princeton University, Princeton, New Jersey 08544
[38]RIKEN BNL Research Center, Upton, New York 11973
[39]Saga University, Saga
[40]University of Science and Technology of China, Hefei
[41]Seoul National University, Seoul
[42]Shinshu University, Nagano
[43]Sungkyunkwan University, Suwon
[44]University of Sydney, Sydney NSW
[45]Tata Institute of Fundamental Research, Bombay
[46]Toho University, Funabashi
[47]Tohoku Gakuin University, Tagajo
[48]Tohoku University, Sendai
[49]Department of Physics, University of Tokyo, Tokyo
[50]Tokyo Institute of Technology, Tokyo
[51]Tokyo Metropolitan University, Tokyo
[52]Tokyo University of Agriculture and Technology, Tokyo
[53]Toyama National College of Maritime Technology, Toyama
[54]University of Tsukuba, Tsukuba
[55]Utkal University, Bhubaneswer
[56]Virginia Polytechnic Institute and State University, Blacksburg, Virginia 24061
[57]Yonsei University, Seoul

Abstract

We report results on studies of CP violation in the three-body charmless decay $B^{\pm} \to K^{\pm}\pi^{\pm}\pi^{\mp}$. Evidence at the 3.9σ level for large direct CP violation in $B^{\pm} \to \rho(770)^0 K^{\pm}$ is found. This is the first evidence for CP violation in a charged meson decay. The analysis is performed using Dalitz analysis technique with a data sample that contains 386 million $B\bar{B}$ pairs collected near the $\Upsilon(4S)$ resonance, with the Belle detector operating at the KEKB asymmetric energy e^+e^- collider.

PACS numbers: 13.25.Hw, 11.30.Er, 14.40.Nd

INTRODUCTION

Decays of B mesons to three-body charmless hadronic final states may provide new possibilities for CP violation searches. In contrast to decays to two-body final states where direct CP violation can only manifest itself as difference in decay rates for B and $\bar{B}$ mesons to charge conjugate final states, in three-body decays it can also be observed as a difference in relative phases between two quasi-two-body channels. A necessary condition for observing direct CP violation in a two-body decay is a non-trivial strong phase difference between the CP-conserving and CP-violating amplitudes contributing to a particular final state. Although this condition (if satisfied) also enhances the sensitivity to CP violation in three-body decays, it is not required in general and direct CP violation in quasi-two-body decays can also be observed with any strong phase difference via the interference with a nearby quasi-two-body or non-resonant amplitude(s). Although direct CP violation has been observed in decays of neutral K mesons [1] and recently in neutral B meson decays [2] no CP violation in decays of charged mesons has been found to date. However, large direct CP violation is expected in some quasi-two-body modes [3]. Several other ideas to study CP violation utilizing decays to three-body final states have been proposed [4, 5, 6, 7].

First results on the amplitude analysis of the $B^\pm \to K^\pm\pi^\pm\pi^\mp$ decay are described in Refs. [8, 9]; the first results on searches for direct CP violation from independent fits of the B^- and B^+ samples are given in Ref. [10, 11]. The analysis of direct CP violation in the decay $B^\pm \to K^\pm\pi^\pm\pi^\mp$ described in this paper is based on a simultaneous fit to B^- and B^+ events. The results are obtained with a data sample of $357\,\text{fb}^{-1}$ containing 386 million $B\bar{B}$ pairs, collected with the Belle detector operating at the KEKB asymmetric-energy e^+e^- collider [12] with a center-of-mass (c.m.) energy at the $\Upsilon(4S)$ resonance (on-resonance data). The beam energies are 3.5 GeV for positrons and 8.0 GeV for electrons. For the study of the $e^+e^- \to q\bar{q}$ continuum background, we use data taken 60 MeV below the $\Upsilon(4S)$ resonance (off-resonance data).

THE BELLE DETECTOR

The Belle detector [13] is a large-solid-angle magnetic spectrometer based on a 1.5 T superconducting solenoid magnet. Charged particle tracking is provided by a silicon vertex

detector and a 50-layer central drift chamber (CDC) that surround the interaction point. Two inner detector configurations were used. A 2.0 cm beampipe and a 3-layer silicon vertex detector was used for the first sample of 152 million $B\bar{B}$ pairs, while a 1.5 cm beampipe, a 4-layer silicon detector and a small-cell inner drift chamber were used to record the remaining 234 million $B\bar{B}$ pairs [14]. The charged particle acceptance covers laboratory polar angles between $\theta = 17^\circ$ and 150°, corresponding to about 92% of the total solid angle in the c.m. frame. The momentum resolution is determined from cosmic rays and $e^+e^- \to \mu^+\mu^-$ events to be $\sigma_{p_t}/p_t = (0.30 \oplus 0.19 p_t)\%$, where p_t is the transverse momentum in GeV/c.

Charged hadron identification is provided by dE/dx measurements in the CDC, an array of 1188 aerogel Čerenkov counters (ACC), and a barrel-like array of 128 time-of-flight scintillation counters (TOF); information from the three subdetectors is combined to form a single likelihood ratio, which is then used in kaon and pion selection. At large momenta (> 2.5 GeV/c) only the ACC and CDC are used to separate charged pions and kaons since here the TOF provides no additional discrimination. Electromagnetic showering particles are detected in an array of 8736 CsI(Tl) crystals (ECL) that covers the same solid angle as the charged particle tracking system. The energy resolution for electromagnetic showers is $\sigma_E/E = (1.3 \oplus 0.07/E \oplus 0.8/E^{1/4})\%$, where E is in GeV. Electron identification in Belle is based on a combination of dE/dx measurements in the CDC, the response of the ACC, and the position, shape and total energy deposition (i.e., E/p) of the shower detected in the ECL. The electron identification efficiency is greater than 92% for tracks with $p_{\rm lab} > 1.0$ GeV/c and the hadron misidentification probability is below 0.3%. The magnetic field is returned via an iron yoke that is instrumented to detect muons and K^0_L mesons. We use a GEANT-based Monte Carlo (MC) simulation to model the response of the detector and determine its acceptance [15].

EVENT RECONSTRUCTION

Charged tracks are selected with a set of track quality requirements based on the number of CDC hits and on the distances of closest approach to the interaction point. We also require that the track momenta transverse to the beam be greater than 0.1 GeV/c to reduce the low momentum combinatorial background. For charged kaon identification we impose a requirement on the particle identification variable which has 86% efficiency and a 7% fake rate from misidentified pions. Charged tracks that are positively identified as electrons or protons are excluded. Since the muon identification efficiency and fake rate vary significantly with the track momentum, we do not veto muons to avoid additional systematic errors.

We identify B candidates using two variables: the energy difference $\Delta E = E_B - E^*_{\rm beam} = (\sum_i \sqrt{c^2\mathbf{p}_i^2 + c^4 m_i^2}) - E^*_{\rm beam}$, and the beam constrained mass $M_{\rm bc} = \frac{1}{c^2}\sqrt{E^{*2}_{\rm beam} - c^2(\sum_i \mathbf{p}_i)^2}$, where the summation is over all particles from a B candidate; $\mathbf{p}_i$ and m_i are their c.m. three-momenta and masses, respectively. The signal ΔE shape is fitted by a sum of two Gaussian functions with a common mean. In fits to the experimental data, we fix the width and the relative fraction of the second Gaussian function from MC simulation. The common mean of the two Gaussian functions and the width of the main Gaussian are floated. The ΔE shape for the $q\bar{q}$ background is parametrized by a linear function. The $M_{\rm bc}$ distribution for the signal events is parametrized by a single Gaussian function. The $M_{\rm bc}$ width is about 3 MeV/c^2 and, in general, does not depend on the final state (unless photons are included in the reconstructed final state). The background shape is parametrized with an empirical function $f(M_{\rm bc}) \propto x\sqrt{1-x^2}\exp[-\xi(1-x^2)]$ [16], where $x = M_{\rm bc}/E^*_{\rm beam}$ and ξ is

a parameter.

BACKGROUND SUPPRESSION

The dominant background is due to $e^+e^- \to\ q\bar{q}$ ($q = u, d, s$ and c quarks) continuum events that have a cross-section about three times larger than that for the $e^+e^- \to \Upsilon(4S) \to B\overline{B}$. This background is suppressed using variables that characterize the event topology. Since the two B mesons produced from an $\Upsilon(4S)$ decay are nearly at rest in the c.m. frame, their decay products are uncorrelated and the event tends to be spherical. In contrast, hadrons from continuum $q\bar{q}$ events tend to exhibit a two-jet structure. We use $\theta_{\rm thr}$, which is the angle between the thrust axis of the B candidate and that of the rest of the event, to discriminate between the two cases. The distribution of $|\cos\theta_{\rm thr}|$ is strongly peaked near $|\cos\theta_{\rm thr}| = 1.0$ for $q\bar{q}$ events and is nearly flat for $B\overline{B}$ events. A Fisher discriminant is utilized for the further suppression of the continuum background. When combined, these two variables reject about 98% of the continuum background in the $B^\pm \to K^\pm\pi^\pm\pi^\mp$ decay while retaining 36% of the signal. A detailed description of the continuum suppression technique can be found in Ref. [6] and references therein.

Another background originates from other B meson decays. We study the $B\overline{B}$ related background using a large sample of MC generated $B\overline{B}$ generic events. Note that charmless hadronic B decays that proceed via $b \to s(d)$ penguin and $b \to u$ tree transitions are not included in the generic MC sample and are generated separately. We find that the dominant $B\overline{B}$ related background to the $K^+\pi^+\pi^-$ final state is due to $B^+ \to \overline{D}^0\pi^+$, $\overline{D}^0 \to K^+\pi^-$ and due to $B^+ \to J/\psi(\psi(2S))K^+$, $J/\psi(\psi(2S)) \to \mu^+\mu^-$ decays. We veto $B^+ \to \overline{D}^0\pi^+$ events by requiring $|M(K\pi) - M_D| > 100$ MeV/c^2. We also veto $B^+ \to \overline{D}^0K^+$, $\overline{D}^0 \to \pi^+\pi^-$ signal by requiring $|M(\pi^+\pi^-) - M_D| > 15$ MeV/c^2. To suppress the background due to π/K misidentification, we also exclude candidates if the invariant mass of any pair of oppositely charged tracks from the B candidate is consistent with the $\bar{D}^0 \to K^+\pi^-$ hypothesis within 25 MeV/c^2 ($\sim 4\sigma$), regardless of the particle identification information. Modes with $J/\psi(\psi(2S))$ in the final state contribute due to muon-pion misidentification; the contribution from the $J/\psi(\psi(2S)) \to e^+e^-$ submode is found to be negligible after the electron veto requirement. We exclude $J/\psi(\psi(2S))$ background by requiring $|M(\pi^+\pi^-)_{\mu^+\mu^-} - M_{J/\psi}| > 70$ MeV/c^2 and $|M(\pi^+\pi^-)_{\mu^+\mu^-} - M_{\psi(2S)}| > 50$ MeV/c^2, with a muon mass assignment used here for the pion candidates. Yet another small but clearly visible background is due to $B^+ \to J/\psi K^+$, $J/\psi \to \mu^+\mu^-$ decay with a complicated series of particle misidentifications; the charged kaon from the B is misidentified as a pion, the μ^+ is misidentified as a kaon and the μ^- as another pion. This background is excluded by applying a veto on the invariant mass of oppositely charged kaon and pion candidates: $|M(K^+\pi^-)_{\mu^+\mu^-} - M_{J/\psi}| > 20$ MeV/c^2. The most significant background from charmless B decays is found to originate from $B^+ \to \eta' K^+$ followed by $\eta' \to \pi^+\pi^-\gamma$. Another contribution comes from $B^+ \to \pi^+\pi^+\pi^-$ decay, where one of the two same charge pions is misidentified as a kaon. Finally, we consider a background from the decay $B^0 \to K^+\pi^-$. Although it does not directly contribute to the ΔE signal region, this background should be taken into account in order to correctly estimate the $q\bar{q}$ component of the background.

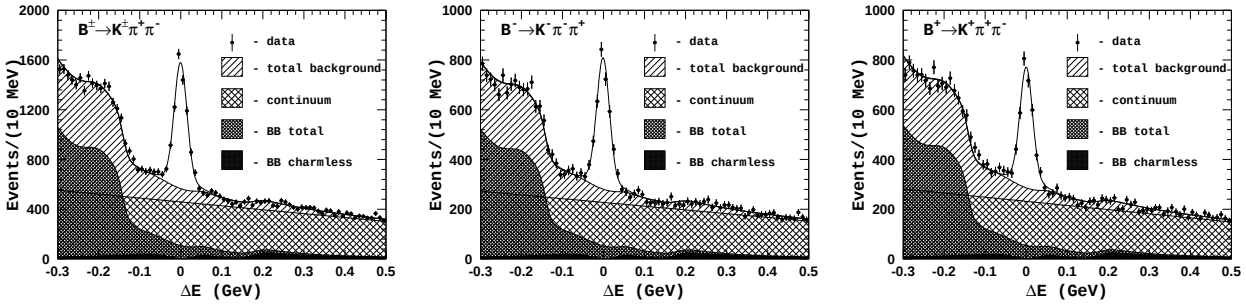

FIG. 1: ΔE distributions for (a) $B^{\pm} \to K^{\pm}\pi^{\pm}\pi^{\mp}$ combined; (b) $B^{-} \to K^{-}\pi^{-}\pi^{+}$ and (c) $B^{+} \to K^{+}\pi^{+}\pi^{-}$ candidate events. Points with error bars are data; the open histogram is the fit result; the hatched histograms are various background components.

THREE-BODY SIGNAL YIELDS

The ΔE distribution for $B^{\pm} \to K^{\pm}\pi^{\pm}\pi^{\mp}$ candidates that pass all the selection requirements are shown in Fig. 1. In the fit to the ΔE distribution we fix the shape and normalization of the charmless $B\overline{B}$ background components from the measured branching fractions [17] and known number of produced $B\overline{B}$ events. For the $B\overline{B}$ generic component we fix only the shape and let the normalization float. The slope and normalization of the $q\bar{q}$ background component are free parameters. Results of the fit are shown in Fig. 1, where different components of the background are shown separately for comparison. There is a large increase in the level of $B\overline{B}$ related background in the region $\Delta E < -0.15$ GeV. This is mainly due to $B \to D\pi$, $D \to K\pi\pi$ decay. This decay mode produces the same final state as the studied process plus one extra pion that is not included in the energy difference calculation. The semileptonic decays $B \to D^{(*)}\pi$, $D \to K\mu\nu_{\mu}$ also contribute due to muon-pion misidentification. The shape of these backgrounds is well described by MC simulation. Results of the ΔE fits are given in Table I.

For the analysis of quasi-two-body intermediate states that contribute to the observed $B^{\pm} \to K^{\pm}\pi^{\pm}\pi^{\mp}$ three-body signal, we define the B signal and sideband regions as shown in Fig. 2. Defined in this way, the $M_{\rm bc} - \Delta E$ sidebands are equivalent to the following sidebands in terms of the three-particle invariant mass $M(K\pi\pi)$ and three-particle momentum $P(K\pi\pi)$:

$$0.05 \text{ GeV}/c^2 < |M(K\pi\pi) - M_B| < 0.10 \text{ GeV}/c^2; \quad P(K\pi\pi) < 0.48 \text{ GeV}/c.$$

TABLE I: Results of the fits of the ΔE distributions.

Final state	σ_1 MeV	σ_2 MeV	Fraction of the main Gaussian	$N_{q\bar{q}}$ (events)	$N_{B\bar{B}}$ (events)	Signal Yield (events)
$B^{-} \to K^{-}\pi^{-}\pi^{+}$	15.6 ± 0.6	35.0 (fixed)	0.84 (fixed)	16932 ± 275	8639 ± 226	2248 ± 79
$B^{+} \to K^{+}\pi^{+}\pi^{-}$	15.0 ± 0.6	35.0 (fixed)	0.84 (fixed)	17268 ± 274	8828 ± 227	2038 ± 76
$B^{\pm} \to K^{\pm}\pi^{\pm}\pi^{\mp}$	15.3 ± 0.5	35.0 (fixed)	0.84 (fixed)	34188 ± 386	17452 ± 320	4286 ± 99

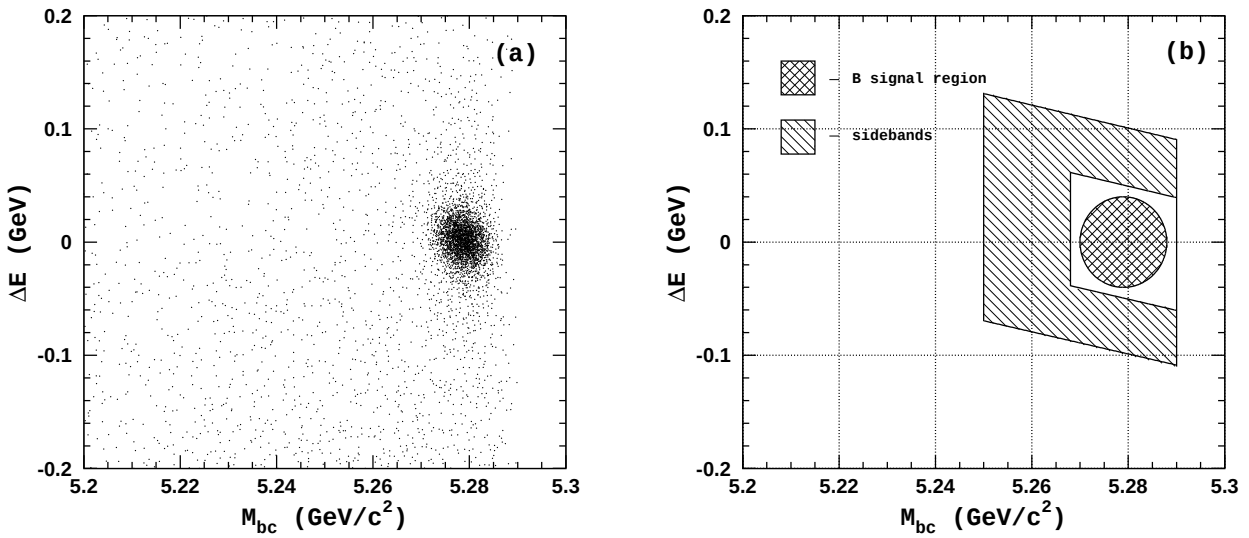

FIG. 2: (a) Two-dimensional ΔE versus $M_{\rm bc}$ plot for the $B^{\pm} \to K^{\pm}\pi^{\pm}\pi^{\mp}$ signal MC events; (b) Definition of the signal and sideband regions on the $M_{\rm bc} - \Delta E$ plane.

and

$$|M(K\pi\pi) - M_B| < 0.10 \text{ GeV}/c^2; \quad 0.48 \text{ GeV}/c < P(K\pi\pi) < 0.65 \text{ GeV}/c.$$

The signal region is defined as an ellipse around the $M_{\rm bc}$ and ΔE mean values:

$$\frac{(M_{\rm bc} - M_B)^2}{(7.5 \text{ MeV}/c^2)^2} + \frac{\Delta E^2}{(40 \text{ MeV})^2} < 1,$$

The efficiency of the requirements that define the signal region is 0.927; the total number of events in the signal region is 7757. The relative fraction of signal events in the B signal region is determined to be 0.512 ± 0.012. There are 27855 events in the sideband region that is about seven times the estimated number of background events in the signal region.

AMPLITUDE ANALYSIS

The amplitude analysis of three-body B meson decay reported here is performed by means of an unbinned maximum likelihood fit. Details of the analysis technique are described in Ref. [8]. One of the important questions that arise in unbinned analysis is the estimation of the goodness-of-fit. As the unbinned maximum likelihood fitting method does not provide a direct way to estimate the quality of the fit, we need a measure to assess how well any given fit represents the data. To do so the following procedure is applied. We first subdivide the entire Dalitz plot into 1 $(\text{GeV}/c^2)^2 \times 1$ $(\text{GeV}/c^2)^2$bins. If the number of events in the bin is smaller than $N_{\rm min} = 25$ it is combined with the adjacent bins until the number of events exceed the minimum required level. After completing this procedure, the entire Dalitz plot is divided into set of bins of varying size, and a χ^2 variable for the multinomial distribution can be calculated as

$$\chi^2 = -2 \sum_{i=1}^{N_{\rm bins}} n_i \ln \left(\frac{p_i}{n_i} \right), \tag{1}$$

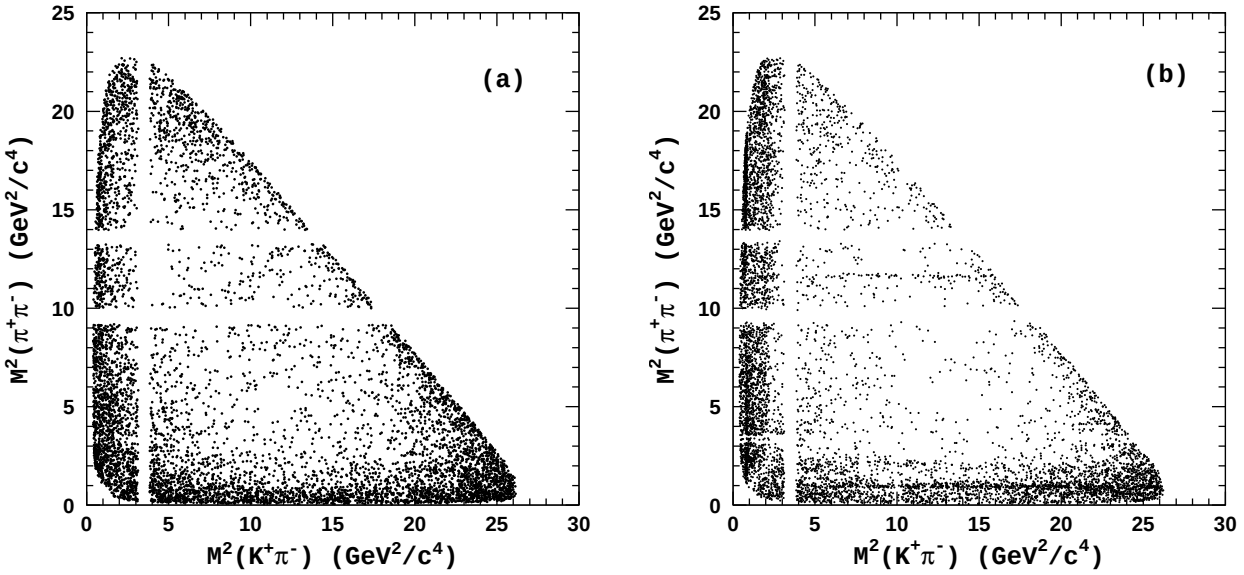

FIG. 3: Dalitz plot for the $K^{\pm}\pi^{\pm}\pi^{\mp}$ events in the (a) $M_{\rm bc} - \Delta E$ sideband region and in (b) B signal region.

where n_i is the number of events observed in i-th bin, and p_i is the number of predicted events from the fit. For a large number of events this formulation becomes equivalent to the usual one. Since we are minimizing the unbinned likelihood function, our "χ^2" variable does not asymptotically follow a χ^2 distribution but it is bounded by a χ^2 variable with $(N_{\rm bins}-1)$ degrees of freedom and a χ^2 variable with $(N_{\rm bins}-k-1)$ degrees of freedom, where k is the number of fit parameters. Because it is bounded by two χ^2 variables, it should be a useful statistic for comparing the relative goodness of fits for different models.

Fitting the Background Shape

Before fitting the Dalitz plot for events in the signal region, we need to determine the distribution of background events. The background density function is determined from an unbinned likelihood fit to the events in the $M_{\rm bc}-\Delta E$ sidebands defined in Fig. 2. Figure 3(a) shows the Dalitz plot for sideband events.

We use the following empirical parameterization to describe the distribution of background events over the Dalitz plot

$$\begin{aligned} B_{K\pi\pi}(s_{13},s_{23}) \;=\; & \alpha_1 e^{-\beta_1 s_{13}} \;+\; \alpha_2 e^{-\beta_2 s_{23}} \;+\; \alpha_3 e^{-\beta_3 s_{12}} \\ & +\; \alpha_4 e^{-(\beta_4 s_{13}+\beta_5 s_{23})} \;+\; \alpha_5 e^{-(\beta_6 s_{13}+\beta_7 s_{12})} \;+\; \alpha_6 e^{-(\beta_8 s_{23}+\beta_9 s_{12})} \\ & +\; \gamma_1 |BW(K^*(892))|^2 \;+\; \gamma_2 |BW(\rho(770))|^2, \end{aligned} \tag{2}$$

where $s_{13} \equiv M^2(K^+\pi^-)$, $s_{23} \equiv M^2(\pi^+\pi^-)$ and α_i ($\alpha_1 \equiv 1.0$), β_i and γ_i are fit parameters; BW is a Breit-Wigner function. The first three terms in Eq. (2) are introduced to describe the background enhancement in the two-particle low invariant mass regions. This enhancement originates mainly from $e^+e^- \to q\bar{q}$ continuum events. Due to the jet-like structure of this background, all three particles in a three-body combination have almost collinear

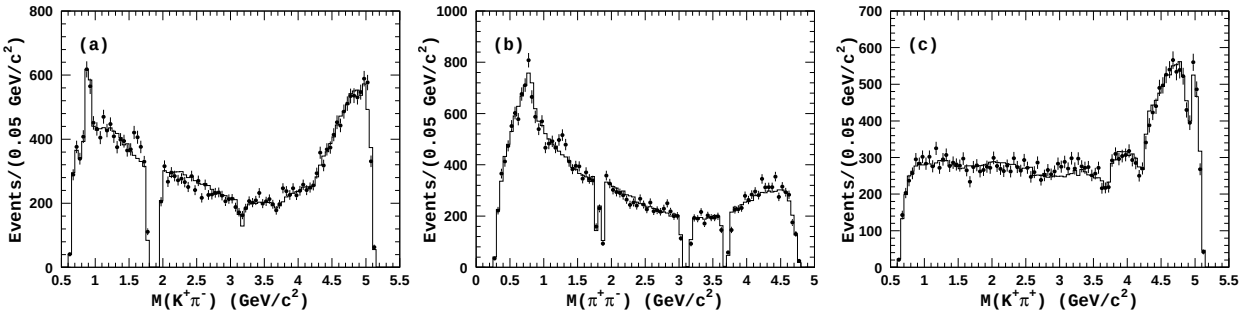

FIG. 4: Results of the best fit to the $K^{\pm}\pi^{\pm}\pi^{\mp}$ events in the $M_{\rm bc} - \Delta E$ sidebands shown as projections onto two-particle invariant mass variables. Points with error bars are data; histograms are fit results.

momenta. Hence, the invariant mass of at least one pair of particles is in the low mass region. In addition, it is often the case that two high momentum particles are combined with a low momentum particle to form a B candidate. In this case there are two pairs with low invariant masses and one pair with high invariant mass. This results in even stronger enhancement of the background in the corners of the Dalitz plot. This is taken into account by terms $4-6$ in Eq. (2). To account for the contribution from real $K^*(892)^0$ and $\rho(770)^0$ mesons, we introduce two more terms in Eq. (2), that are (non-interfering) squared Breit-Wigner amplitudes, with masses and widths fixed at world average values [17].

The projections of the data and fits for the background events are shown in Fig. 4. The $\chi^2/N_{\rm bins}$ value of the fit is 127.6/120.

Fitting the $B^{\pm} \to K^{\pm}\pi^{\pm}\pi^{\mp}$ Signal

The Dalitz plot for $K^{\pm}\pi^{\pm}\pi^{\mp}$ events in the signal region is shown in Fig. 3(b). There are 7757 events in the signal region that satisfy all the selection requirements. As found in Ref. [8] the $B^+ \to K^+\pi^+\pi^-$ decay is well described by a matrix element that is a coherent sum of $K^*(892)^0\pi^+$, $K_0^*(1430)^0\pi^+$, $\rho(770)^0K^+$, $f_0(980)K^+$, $f_X(1300)K^+$, $\chi_{c0}K^+$ quasi-two-body channels and a non-resonant amplitude. The $f_X(1300)K^+$ channel is added in order to describe an excess of signal events at $M(\pi^+\pi^-) \simeq 1.3$ GeV/c^2. With current statistics, the contribution of $f_2(1270)K^+$ is found to be significant, but not sufficient to fully explain the excess of signal events in this mass region. In this analysis we modify the model by adding two more quasi-two-body channels: $f_2(1270)K^+$ and $\omega(782)K^+$ and change the parameterization of the $f_0(980)$ lineshape from a standard Breit-Wigner function to a coupled channel Breit-Wigner also known as Flatté parametrization [18]. Although the $\omega(782) \to \pi^+\pi^-$ branching fraction is only $(1.70 \pm 0.27)\%$ [17], the $\omega(782)$ natural width is rather narrow. As a result a numerical factor of $\Gamma(\rho(770)^0)/\Gamma(\omega(782)) \sim 18$ is introduced in the $B \to \omega(782)K$ amplitude (relative to the $B \to \rho(770)K$ amplitude) that compensates the smallness of the $\omega(782) \to \pi^+\pi^-$ branching. As the independently measured $B^{\pm} \to \omega(782)K^{\pm}$ branching fraction [19] is comparable to that for $B^{\pm} \to \rho(770)^0K^{\pm}$, the interference between these two amplitudes might significantly distort the $\rho(770)^0$ lineshape. Finally, for CP violation studies the amplitude for each quasi-two-body channel is modified to include two components: one that is independent of the sign of the B charge and a component that changes sign with

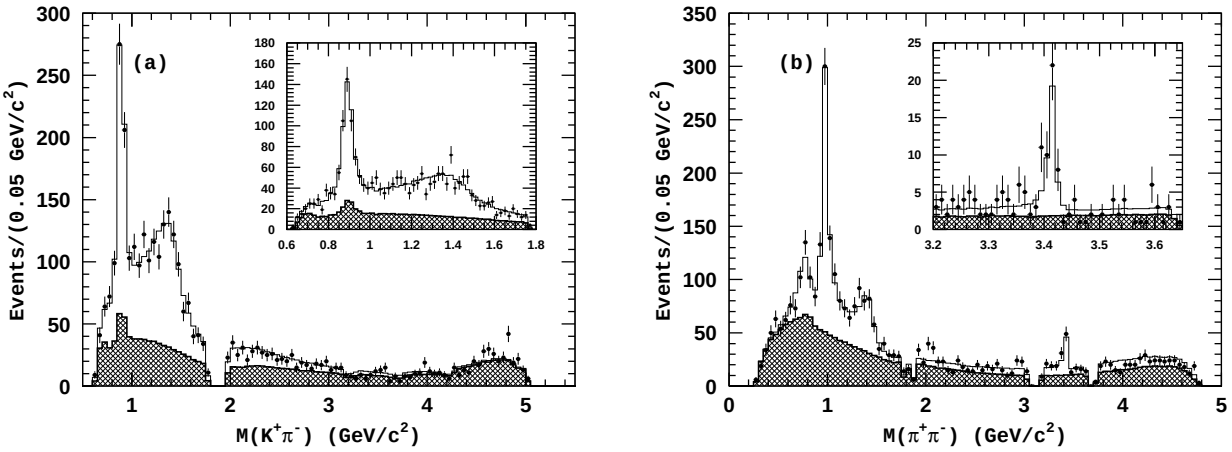

FIG. 5: Results of the fit to $K^{\pm}\pi^{\pm}\pi^{\mp}$ events in the signal region. Points with error bars are data, the open histograms are the fit result and hatched histograms are the background components. Inset in (a) shows the $K^*(892) - K_0^*(1430)$ mass region in 20 MeV/c^2 bins. Inset in (b) shows the χ_{c0} mass region in 10 MeV/c^2 bins.

the charge of the B meson. The resulting decay amplitude reads as

$$\begin{aligned}
&\mathcal{M}(B^{\pm} \to K^{\pm}\pi^{\pm}\pi^{\mp}) = \\
&= a_{K^*} e^{i\delta_{K^*}}(1 \pm b_{K^*} e^{i\varphi_{K^*}})\mathcal{A}(K^*(892)^0) + a_{K_0^*} e^{i\delta_{K_0^*}}(1 \pm b_{K_0^*} e^{i\varphi_{K_0^*}})\mathcal{A}(K_0^*(1430)^0) \\
&+ \; a_{\rho} e^{i\delta_{\rho}}(1 \pm b_{\rho} e^{i\varphi_{\rho}})\mathcal{A}(\rho(770)^0) + a_{\omega} e^{i\delta_{\omega}}(1 \pm b_{\omega} e^{i\varphi_{\omega}})\mathcal{A}(\omega(782)) \\
&+ \; a_{f_0} e^{i\delta_{f_0}}(1 \pm b_{f_0} e^{i\varphi_{f_0}})\mathcal{A}_{\rm Flatte}(f_0(980)) + a_{f_2} e^{i\delta_{f_2}}(1 \pm b_{f_2} e^{i\varphi_{f_2}})\mathcal{A}(f_2(1270)) \\
&+ \; a_{f_X} e^{i\delta_{f_X}}(1 \pm b_{f_X} e^{i\varphi_{f_X}})\mathcal{A}(f_X) + a_{\chi_{c0}} e^{i\delta_{\chi_{c0}}}(1 \pm b_{\chi_{c0}} e^{i\varphi_{\chi_{c0}}})\mathcal{A}(\chi_{c0}) \\
&+ \; \mathcal{A}_{\rm nr}(K^{\pm}\pi^{\pm}\pi^{\mp})
\end{aligned} \tag{3}$$

with the non-resonant amplitude $\mathcal{A}_{\rm nr}$ parametrized by an empirical function

$$\mathcal{A}_{\rm nr}(K^{\pm}\pi^{\pm}\pi^{\mp}) = a_1^{\rm nr} e^{-\alpha s_{13}} e^{i\delta_1^{\rm nr}} + a_2^{\rm nr} e^{-\alpha s_{23}} e^{i\delta_2^{\rm nr}}, \tag{4}$$

where $s_{13} \equiv M^2(K^{\pm}\pi^{\mp})$, $s_{23} \equiv M^2(\pi^+\pi^-)$. Note that alternative parameterizations of the non-resonant amplitude possible [8, 11]. The amplitudes a_i and b_i, relative phases δ_i and φ_i, mass, $g_{\pi\pi}$ and g_{KK} of the $f_0(980)$, mass and width of the $f_X(1300)$, and parameter α of the non-resonant amplitude are fit parameters. With such a parameterization of the amplitude, the CP violating asymmetry A_{CP} for a particular quasi-two-body channel can be calculated as

$$A_{CP}(f) = \frac{\mathcal{B}(B^- \to f^-) - \mathcal{B}(B^+ \to f^+)}{\mathcal{B}(B^- \to f^-) + \mathcal{B}(B^+ \to f^+)} = -\frac{2b\cos\varphi}{1+b^2}. \tag{5}$$

To reduce the number of free fit parameters, we fit the data in two steps. First we fix all $b_i = 0$ and fit the data assuming no CP violation. From this fit we determine the parameters of the $f_X(1300)$ ($M(f_X(1300)) = 1.449 \pm 0.013$ GeV/c^2, $\Gamma(f_X(1300)) = 0.126 \pm 0.025$ GeV/c^2), $f_0(980)$ ($M(f_0(980) = 0.950 \pm 0.009$ GeV/c^2, $g_{\pi\pi} = 0.23 \pm 0.05$, $g_{KK} = 0.73 \pm 0.30$) and the parameter of the non-resonant amplitude ($\alpha = 0.195 \pm 0.018$). We then fix these parameters and repeat the fit to data with b_i and φ_i floating. In addition,

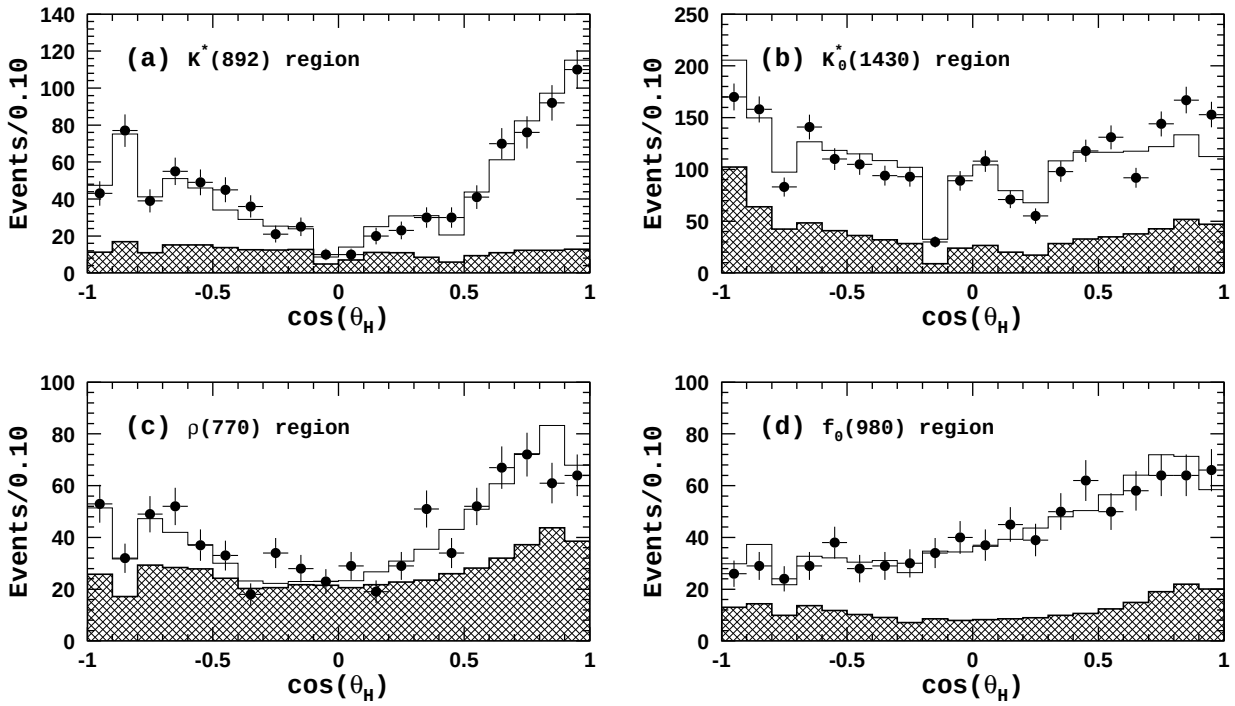

FIG. 6: Helicity angle distributions for $K^{\pm}\pi^{\pm}\pi^{\mp}$ events in different regions: (a) $K^*(892)^0$ ($0.82\ \text{GeV}/c^2 < M(K^+\pi^-) < 0.97\ \text{GeV}/c^2$); (b) $K_0^*(1430)$ ($1.00\ \text{GeV}/c^2 < M(K^+\pi^-) < 1.76\ \text{GeV}/c^2$); (c) $\rho^0(770)$ ($0.60\ \text{GeV}/c^2 < M(\pi^+\pi^-) < 0.90\ \text{GeV}/c^2$) and (d) $f_0(980)$ ($0.90\ \text{GeV}/c^2 < M(\pi^+\pi^-) < 1.06\ \text{GeV}/c^2$). Points with error bars are data, the open histogram is the fit result and the hatched histogram is the background component.

we also assume no CP violation in $B^{\pm} \to \omega(782)K^{\pm}$ and for the non-resonant amplitude. Possible effects of these assumptions are studied and considered in the final results as a part of the model uncertainty.

The numerical values of the fit parameters are given in Table II. The $\chi^2/N_{\rm bins}$ value of the fit is 182.5/141 with $k = 32$ fit parameters. Fit projections and the data are shown in Fig. 5. Figure 6 shows helicity angle distributions for several regions, where the helicity angle is defined as the angle between the direction of flight of the π^- in the $h^+\pi^-$ rest frame and the direction of B^+ candidate in the $h^+\pi^-$ rest frame. Gaps visible in Fig. 6 are due to vetoes applied on invariant masses of two-particle combinations. All plots shown in Figs. 5 and 6 demonstrate good agreement between data and the fit.

The statistical significance of the asymmetry quoted in Table II is calculated as $\sqrt{-2\ln(\mathcal{L}_0/\mathcal{L}_{\rm max})}$, where $\mathcal{L}_{\rm max}$ and $\mathcal{L}_0$ denote the maximum likelihood with nominal fit and with the asymmetry fixed at zero, respectively. The only channel where the statistical significance of the CP asymmetry exceeds the 3σ level is $B^{\pm} \to \rho(770)^0 K^{\pm}$. Figures 7(a,b) show the $\pi^+\pi^-$ invariant mass distributions for the $\rho(770)^0 - f_0(980)$ mass region separately for B^- and B^+ events. The effect is even more apparent when the $M(\pi^+\pi^-)$ distribution for the two helicity angle regions ($\cos\theta_H^{\pi\pi} < 0$ and $\cos\theta_H^{\pi\pi} > 0$) shown in Fig. 7(c-f) are compared.

TABLE II: Results of the best fit to $K^{\pm}\pi^{\pm}\pi^{\mp}$ events in the B signal region. The first quoted error is statistical and the second is the model dependent uncertainty. The quoted significance is statistical only.

Channel	CP averaged fraction, %	δ, degrees	b	φ, degrees	A_{CP}, %	Significance, σ
$K^*(892)^0\pi^{\pm}$	$13.0 \pm 0.8^{+0.5}_{-0.7}$	0 (fixed)	$0.078 \pm 0.033^{+0.012}_{-0.003}$	$-18 \pm 44^{+5}_{-13}$	$-14.9 \pm 6.4^{+0.8}_{-0.8}$	2.6
$K_0(1430)^0\pi^{\pm}$	$65.5 \pm 1.5^{+2.2}_{-3.9}$	$55 \pm 4^{+1}_{-5}$	$0.069 \pm 0.031^{+0.010}_{-0.008}$	$-123 \pm 16^{+4}_{-5}$	$+7.5 \pm 3.8^{+2.0}_{-0.9}$	2.7
$\rho(770)^0K^{\pm}$	$7.85 \pm 0.93^{+0.64}_{-0.59}$	$-21 \pm 14^{+14}_{-19}$	$0.28 \pm 0.11^{+0.07}_{-0.09}$	$-125 \pm 32^{+10}_{-85}$	$+30 \pm 11^{+11}_{-4}$	3.9
$\omega(782)K^{\pm}$	$0.15 \pm 0.12^{+0.03}_{-0.02}$	$100 \pm 31^{+38}_{-21}$	0 (fixed)	–	–	–
$f_0(980)K^{\pm}$	$17.7 \pm 1.6^{+1.1}_{-3.3}$	$67 \pm 11^{+10}_{-11}$	$0.30 \pm 0.19^{+0.05}_{-0.10}$	$-82 \pm 8^{+2}_{-2}$	$-7.7 \pm 6.5^{+4.1}_{-1.6}$	1.6
$f_2(1270)K^{\pm}$	$1.52 \pm 0.35^{+0.22}_{-0.37}$	$140 \pm 11^{+18}_{-7}$	$0.37 \pm 0.17^{+0.11}_{-0.03}$	$-24 \pm 29^{+14}_{-20}$	$-59 \pm 22^{+3}_{-3}$	2.7
$f_X(1300)K^{\pm}$	$4.14 \pm 0.81^{+0.31}_{-0.30}$	$-141 \pm 10^{+8}_{-9}$	$0.12 \pm 0.17^{+0.04}_{-0.07}$	$-77 \pm 56^{+88}_{-43}$	$-5.4 \pm 16.5^{+10.3}_{-2.4}$	1.0
Non-Res.	$34.0 \pm 2.2^{+2.1}_{-1.8}$	$\delta_1^{\rm nr} = -11 \pm 5^{+3}_{-3}$ $\delta_2^{\rm nr} = 185 \pm 20^{+62}_{-19}$	0 (fixed)	–	–	–
$\chi_{c0}K^{\pm}$	$1.12 \pm 0.12^{+0.24}_{-0.08}$	$-118 \pm 24^{+37}_{-38}$	$0.15 \pm 0.35^{+0.08}_{-0.07}$	$-77 \pm 94^{+154}_{-11}$	$-6.5 \pm 19.6^{+2.9}_{-1.4}$	0.7

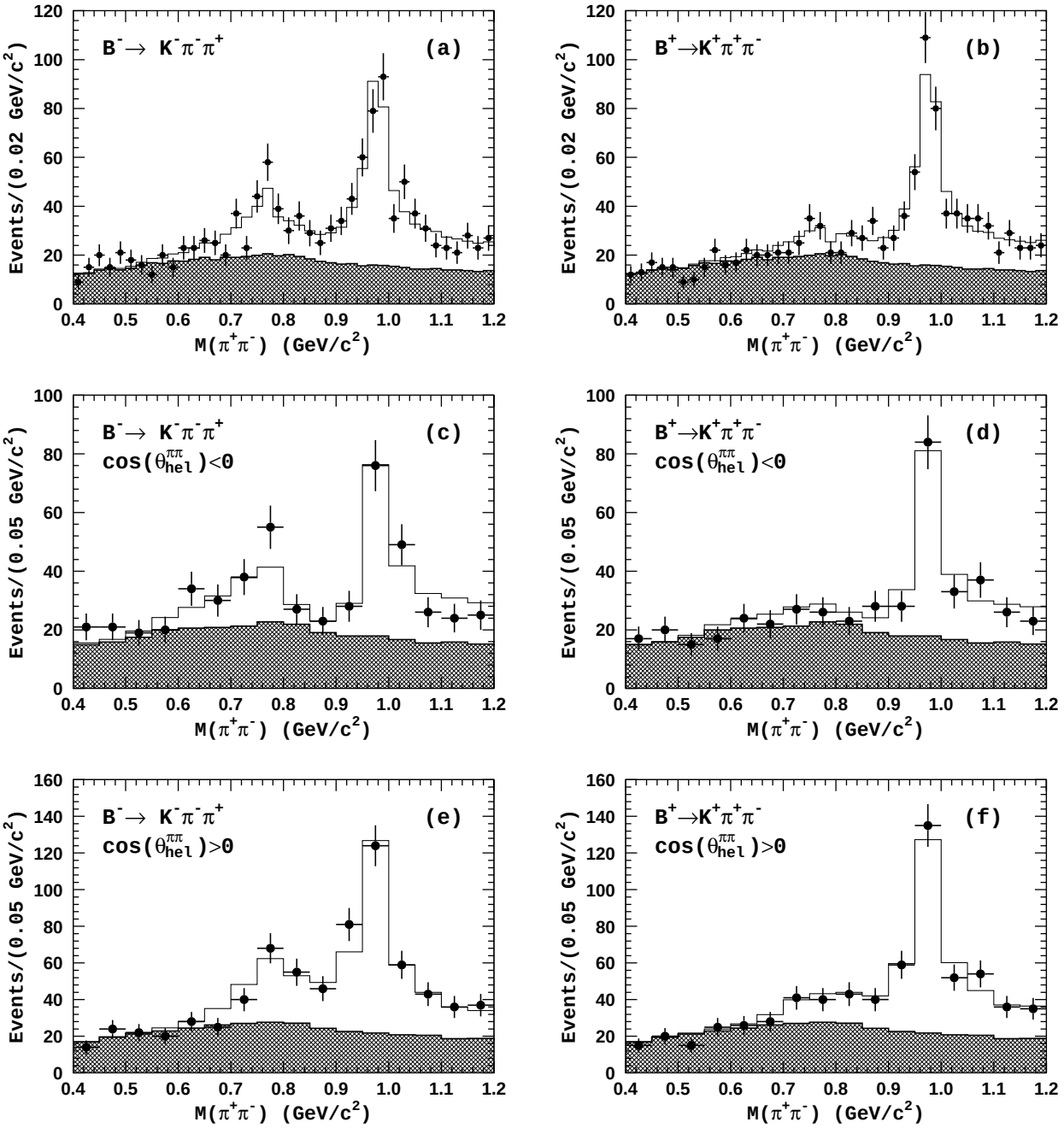

FIG. 7: $M(\pi^+\pi^-)$ mass spectra for B^- (left column) and B^+ (right column) for different helicity regions: (a,b) no helicity cuts; (c,d) $\cos\theta_H^{\pi\pi} < 0$; (e,f) $\cos\theta_H^{\pi\pi} > 0$; Points with error bars are data, the open histogram is the fit result and the hatched histogram is the background component.

SYSTEMATIC & MODEL UNCERTAINTIES

The dominant sources of systematic error are listed in Table III. The systematic uncertainty in charged track reconstruction is estimated using partially reconstructed $D^* \to D\pi$ events and from comparison of the ratio of $\eta \to \pi^+\pi^-\pi^0$ to $\eta \to \gamma\gamma$ events in data and MC. The uncertainty from the particle identification efficiency is estimated using pure samples of

TABLE III: List of systematic errors (in percent) for the three-body $B^{\pm} \to K^{\pm}\pi^{\pm}\pi^{\mp}$ branching fraction.

Source	Error
Charged track reconstruction	3.0
PID	4.5
Event Shape requirements	2.5
Signal yield extraction	3.9
Model	1.2
MC statistics	1.0
Luminosity measurement	1.0
Total	7.4

kaons and pions from $D^0 \to K^-\pi^+$ decays, where the D^0 flavor is tagged using $D^{*+} \to D^0\pi^+$ decays. The systematic uncertainty due to requirements on event shape variables is estimated from a comparison of the $|\cos\theta_{\rm thr}|$ and $\mathcal{F}$ distributions for signal MC events and $B^+ \to \overline{D}^0\pi^+$ events in the data. We estimate the uncertainty due to the signal ΔE shape parameterization by varying the parameters of the fitting function within their errors. The uncertainty in the background parameterization is estimated by varying the relative fraction of the $B\overline{B}$ background component and the slope of the $q\bar{q}$ background function within their errors. Reconstruction efficiency is determined using MC events distributed over phase space according to the matrix element corresponding to the best fit to data. The relevant systematic uncertainty is estimated to be at the level of one percent. Finally, to account for variations in reconstruction efficiency due to modifications in the detector setup and due to non-uniform data-taking conditions (mainly beam related background conditions), we generate signal events with background events embedded. Background events are recorded with random triggers for each experiment. Signal MC events are generated for each experiment with statistics proportional to experimental data. The overall systematic uncertainty for the three-body branching fraction is 7.4%.

Note that in asymmetry calculation most of these systematic uncertainties cancel. The few remaining sources are listed in Table IV. Systematic uncertainty due to possible asymmetry in background from charmless B decays is estimated by introducing an asymmetry

TABLE IV: List of systematic errors for CP violating asymmetry.

Source	δA_{CP}
Rare background	
$\rho^0\pi^{\pm}$	$+0.003/-0.004$
$\eta' K^{\pm}$	$+0.001/-0.001$
$K^{\pm}\pi^{\mp}$	$+0.004/-0.004$
Detector asymmetry	$+0.023/-0.023$
Signal yield extraction	$+0.011/-0.011$
Total	$+0.031/-0.029$

equal to experimentally measured central value [19] increased by one standard deviation to each charmless background component one by one and refitting the data. The possible bias due to intrinsic detector asymmetry in reconstruction of tracks of different charges is estimated using $B \to D\pi$ events in data.

To estimate the model dependent uncertainty in the branching fractions and asymmetries for individual quasi-two-body intermediate states, we vary the default model and repeat the fit to data. Namely, we add one additional quasi-two-body channel which is either $K^*(1410)^0\pi^+$, $K^*(1680)^0\pi^+$, or $K_2^*(1430)^0\pi^+$ or remove $\omega(782)K^+$ or $f_2(1270)K^+$ channel from the default model, use different assumptions on the spin of the $f_X(1300)$ state and use different parameterizations of the non-resonant amplitude. For estimation of the model uncertainty in charge asymmetries for individual quasi-two-body channels in addition to model variations we fit the data with different assumptions on CP violation in different channels. Finally, we check the consistency of the A_{CP} results with those obtained from independent fits of B^- and B^+ subsamples.

BRANCHING FRACTION & CHARGE ASYMMETRY RESULTS

In the preceding section we determined the relative fractions of various quasi-two-body intermediate states in the three-body $B^\pm \to K^\pm\pi^\pm\pi^\mp$ decay. To translate those numbers into absolute branching fractions, we first need to determine the branching fraction for the three body decay. To determine the reconstruction efficiency, we use MC simulation where events are distributed over the phase space according to the matrix elements obtained from the best fit to data. The corresponding reconstruction efficiency is $(22.4 \pm 0.2)\%$. Results of the branching fraction and CP-violating asymmetry calculations are summarized in Table V.

TABLE V: Summary of branching fraction results. The first quoted error is statistical, the second is systematic and the third is the model uncertainty.

Mode	$\mathcal{B}(B^+ \to Rh^+ \to K^+\pi^+\pi^-)$ $\times 10^6$	$\mathcal{B}(B^+ \to Rh^+)$ $\times 10^6$	A_{CP}, %
$K^\pm\pi^\pm\pi^\mp$ Charmless	–	$48.8 \pm 1.1 \pm 3.6$	$4.9 \pm 2.6 \pm 3.0$
$K^*(892)^0[K^+\pi^-]\pi^+$	$6.45 \pm 0.43 \pm 0.48^{+0.25}_{-0.35}$	$9.67 \pm 0.64 \pm 0.72^{+0.37}_{-0.52}$	$-14.9 \pm 6.4 \pm 3.0^{+0.8}_{-0.8}$
$K_0^*(1430)[K^+\pi^-]\pi^+$	$32.0 \pm 1.0 \pm 2.4^{+1.1}_{-1.9}$	$51.6 \pm 1.7 \pm 6.8^{+1.8}_{-3.1}$	$+7.6 \pm 3.8 \pm 3.0^{+2.0}_{-0.9}$
$\rho(770)^0[\pi^+\pi^-]K^+$	$3.89 \pm 0.47 \pm 0.29^{+0.32}_{-0.29}$	$3.89 \pm 0.47 \pm 0.29^{+0.32}_{-0.29}$	$+30 \pm 11 \pm 3.0^{+11}_{-4}$
$f_0(980)[\pi^+\pi^-]K^+$	$8.78 \pm 0.82 \pm 0.65^{+0.55}_{-1.64}$	–	$-7.7 \pm 6.5 \pm 3.0^{+4.1}_{-1.6}$
$f_2(1270)[\pi^+\pi^-]K^+$	$0.75 \pm 0.17 \pm 0.06^{+0.11}_{-0.18}$	$1.78 \pm 0.41 \pm 0.14^{+0.26}_{-0.43}$	$-59 \pm 22 \pm 3.0^{+3}_{-3}$
Non-resonant	–	$16.9 \pm 1.3 \pm 1.3^{+1.1}_{-0.9}$	–
$\chi_{c0}[\pi^+\pi^-]K^+$	$0.56 \pm 0.06 \pm 0.04^{+0.12}_{-0.04}$	$112 \pm 12 \pm 18^{+24}_{-8}$	$-6.5 \pm 19.6 \pm 3.0^{+2.9}_{-1.4}$

DISCUSSION & CONCLUSION

With a 357 fb^{-1} data sample collected with the Belle detector, we made the first analysis of direct CP violation in the three-body charmless decay $B^\pm \to K^\pm\pi^\pm\pi^\mp$. Results on

branching fraction and CP-violating asymmetry calculations are summarized in Table V. In all except the $B^{\pm} \to \rho(770)^0 K^{\pm}$ channel the measured asymmetry is below 3σ statistical significance. Evidence for large direct CP violation the decay $B^{\pm} \to \rho(770)^0 K^{\pm}$ is found in agreement with our results obtained with 253 fb^{-1} [10] and with results by BaBar [11]. This is also in agreement with some theoretical predictions [3]. The statistical significance of the asymmetry observed in $B^{\pm} \to \rho(770)^0 K^{\pm}$ is 3.9σ. Depending on the model used to fit the data the significance varies from 3.7σ to 4.0σ. If confirmed with a larger data sample, this would be the first observation of CP violation in the decay of a charged meson.

Acknowledgments

We thank the KEKB group for the excellent operation of the accelerator, the KEK cryogenics group for the efficient operation of the solenoid, and the KEK computer group and the National Institute of Informatics for valuable computing and Super-SINET network support. We acknowledge support from the Ministry of Education, Culture, Sports, Science, and Technology of Japan and the Japan Society for the Promotion of Science; the Australian Research Council and the Australian Department of Education, Science and Training; the National Science Foundation of China under contract No. 10175071; the Department of Science and Technology of India; the BK21 program of the Ministry of Education of Korea and the CHEP SRC program of the Korea Science and Engineering Foundation; the Polish State Committee for Scientific Research under contract No. 2P03B 01324; the Ministry of Science and Technology of the Russian Federation; the Ministry of Higher Education, Science and Technology of the Republic of Slovenia; the Swiss National Science Foundation; the National Science Council and the Ministry of Education of Taiwan; and the U.S. Department of Energy.

[1] J.R. Batley *et al.* (NA48 Collaboration), Phys. Lett. **B544**, 97 (2002); A. Alavi-Harati *et al.* (KTeV Collaboration), Phys. Rev. **D67**, 012005 (2003).

[2] B. Aubert *et al.* (BaBar Collaboration), Phys. Rev. Lett. **93**, 131801 (2004); Y. Chao *et al.* (Belle Collaboration), Phys. Rev. Lett. **93**, 191802 (2004).

[3] See for example: M. Beneke and M. Neubert, Nucl. Phys. **B675**, 333 (2003); C.-W. Chiang, M. Gronau, Z. Luo, J. Rosner, and D. Suprun, Phys. Rev. **D69**, 034001 (2004) and references therein.

[4] G. Eilam, M. Gronau and R. R. Mendel, Phys. Rev. Lett. **74**, 4984 (1995); S. Fajfer, R. J. Oakes, and T. N. Pham, Phys. Lett. **B539**, 67 (2002).

[5] N. G. Deshpande, N. Sinha and R. Sinha, Phys. Rev. Lett. **90**, 061802 (2003); M. Gronau, Phys. Rev. Lett. **91**, 139101 (2003).

[6] A. Garmash *et al.* (Belle Collaboration), Phys. Rev. **D69**, 012001 (2004).

[7] T. Gershon and M. Hazumi, Phys. Lett. **B596**, 163 (2004).

[8] A. Garmash *et al.* (Belle Collaboration), Phys. Rev. **D71**, 092003 (2005).

[9] B. Aubert *et al.* (BaBar Collaboration), hep-ex/0408032.

[10] A. Garmash *et al.* (Belle Collaboration), hep-ex/0505048.

[11] B. Aubert *et al.* (BaBar Collaboration), hep-ex/0507004, Submitted to Phys. Rev. D.

[12] S. Kurokawa, Nucl. Instr. and Meth. **A499**, 1 (2003).

[13] A. Abashian *et al.*, Nucl. Instr. and Meth. **A479**, 117 (2002).
[14] Y. Ushiroda (Belle SVD2 Group), Nucl. Instr. and Meth. **A511**, 6 (2003).
[15] R. Brun *et al.*, GEANT 3.21, CERN Report DD/EE/84-1, 1984.
[16] H. Albrecht *et al.* (ARGUS Collaboration), Phys. Lett. **B229**, 304 (1989).
[17] S. Eidelman *et al.* (Particle Data Group), Phys. Lett. **B592**, 1 (2004).
[18] S.M. Flatté, Phys. Lett. **B63**, 224 (1976).
[19] Heavy Flavor Averaging Group, hep-ex/0505100, and updates available at `http://www.slac.stanford.edu/xorg/hfag/`.